J Nanopart Res (2012) 14:746
DOI 10.1007/s11051-012-0746-3

RESEARCH PAPER

The film thickness dependent thermal stability of Al_2O_3:Ag thin films as high-temperature solar selective absorbers

Xiudi Xiao · Gang Xu · Bin Xiong · Deming Chen · Lei Miao

Received: 16 August 2011 / Accepted: 17 January 2012 / Published online: 9 February 2012

Abstract The monolayer Al_2O_3:Ag thin films were prepared by magnetron sputtering. The microstructure and optical properties of thin film after annealing at 700 °C in air were characterized by transmission electron microscopy, X-ray diffraction, X-ray photoelectron spectroscopy, and spectrophotometer. It revealed that the particle shape, size, and distribution across the film were greatly changed before and after annealing. The surface plasmon resonance absorption and thermal stability of the film were found to be strongly dependent on the film thickness, which was believed to be associated with the evolution process of particle diffusion, agglomeration, and evaporation during annealing at high temperature. When the film thickness was smaller than 90 nm, the film SPR absorption can be attenuated until extinct with increasing annealing time due to the evaporation of Ag particles. While the film thickness was larger than 120 nm, the absorption can keep constant even after annealing for 64 h due to the agglomeration of Ag particles. On the base of film thickness results, the multilayer Al_2O_3:Ag solar selective thin films were prepared and the thermal stability test illustrated that the solar selectivity of multilayer films with absorbing layer thickness larger than 120 nm did not degrade after annealing at 500 °C for 70 h in air. It can be concluded that film thickness is an important factor to control the thermal stability of Al_2O_3:Ag thin films as high-temperature solar selective absorbers.

Keywords Al_2O_3:Ag thin films · Solar selective absorbers · SPR absorption · Thermal stability · Energy conversion

X. Xiao · G. Xu (✉) · B. Xiong · D. Chen · L. Miao
Key Laboratory of Renewable Energy and Gas Hydrates, Guangzhou Institute of Energy Conversion, Chinese Academy of Sciences, Guangzhou 510640, People's Republic of China
e-mail: xiudixiao@163.com; xugang@ms.giec.ac.cn

Introduction

Solar selective absorber, as one of the most key components to transfer solar energy to heat energy, known so far are mostly cermet materials, namely, metal-dielectric composites (Granqvist 1991). The highly absorbing metal-dielectric composite is composed of fine metal particles in a dielectric or ceramic matrix. It offers high degree flexibility and the solar selectivity can be optimized by proper choice of constituents, film thickness, and concentration, size, and shape of metal particles (Kennedy 2002). For the high temperature (higher than 500 °C) use of solar energy, the constituent of cermet is the key point.

Alumina (Al_2O_3) is one of common matrix for small metallic particles in solar absorbers due to its stability at high temperature and transparency in long wavelength

region. With the appropriate concentration of metallic particles and correct film thickness, this cermet layer has good solar selective properties (Blain et al. 1985; Uchino et al. 1979; Niklasson and Granqvist 1984; Wackelgard et al. 1990). Nickel-pigmented alumina is a classic example for selective system (Salmi et al. 2000). However, among these cermet absorbers, humidity and the oxidation of metallic particles at high temperature can greatly increase the emissivity and causes degradation of solar selectivity, which restricts their application in the high temperature. Although different methods are proposed to prevent the degradation of metal nanoparticles, such as sealing in vacuum (Peterson and Ramsey 1975), protective layer as well as antireflective layer (Sathiaraj et al. 1990) which can not solve the problem radically.

Silver (Ag), as one of noble metals, has attracted considerable interest for their unique optical properties known as surface plasmon resonance (SPR). SPR is excited when the incident light with a specific wavelength interacts with the metal nanoparticles to create the collective oscillation of conduction electrons. It is accompanied by wavelength-selective photon absorption and resonant Mie scattering and by a dramatic enhancement of the local electromagnetic field in the vicinity of the nanoparticles (Granqvist 1991; Kelly et al. 2003; Murray and Barnes 2007). Taking advantage of the SPR of Ag nanoparticles, the concentration of metallic particles in cermet can be reduced, which can immediately decrease emissivity of cermet solar absorbers at high temperature and metal cost. Moreover, Ag has superior stability at high temperature due to the decomposition of Ag oxides (Ag_2O) around 300 °C (Cai et al. 1998; Bi et al. 2002), which indicates that Ag is a good candidate metal for high temperature cermet solar absorber.

$$Ag_2O \xrightarrow{300\,^{\circ}C} Ag + O_2 \quad (1)$$

Recently, Barshilia et al. (2011) have prepared the high solar selectivity Al_2O_3:Ag absorber and proved that the degradation of Al_2O_3:Ag thin film in vacuum at 400 °C is resulted from the defragmentation of Ag nanoparticles inside the alumina matrix. We have previously proved that the multilayer Al_2O_3:Ag absorbers have superior solar selectivity in atmosphere (Wang et al. 2011). In the present paper, the microstructure and optical properties of monolayer Al_2O_3:Ag thin film before and after annealing were investigated. Interestingly, it was found that the thermal stability of monolayer film was strongly dependent on the film thickness, which was believed to be associated with the evolution process of particle diffusion, agglomeration and evaporation during annealing at high temperature. Moreover, the multilayer Al_2O_3:Ag thin film as solar absorbers was also prepared to prove the film thickness dependent thermal stability.

Experimental

Sample preparation

Al_2O_3:Ag thin films were fabricated by magnetron sputtering two targets of Ag (99.99% purity) and Al_2O_3 (99.8% purity) in Ar at room temperature, respectively. The sputtering pressure was kept constant at 1 Pa and the rf powers were set as 10 W for Ag and 120 W for Al_2O_3, respectively. The deposition rate for Ag and Al_2O_3 are equivalent at the designed rf powers. Thus, the volume fraction of Ag in Al_2O_3 matrix is about 0.5. Fused quartz was used as substrate. The thickness of thin film was recorded with a quartz crystal oscillator. To investigate the thickness dependent properties, samples with nominal thickness about 60, 90, 120, and 150 nm, respectively, were prepared. For simplicity, samples with different thickness were labeled as A (60 nm), B (90 nm), C (120 nm), and D (150 nm), respectively. After deposition, samples were heated in the muffle with air atmosphere at 700 °C for 4, 8, 12, 16, 20, 48, 56, 64, 80 h, respectively. Generally, the solar absorber is a multilayer structure. Thus, the multilayer thin film with four layers was also prepared to prove the thickness dependent thermal stability. The thin film consisted of an Al_2O_3 antireflection layer (AR), an absorbing layer composed of two homogenous Al_2O_3:Ag cermet layers (a low-metal-volume fraction (LMVF) cermet layer on a high-metal-volume fraction (HMVF)) and a Ag infrared reflector layer. The concentration of Ag in LMVF layer and HMVF layer are 0.09 and 0.5, respectively. Nominal thickness of absorbing layer was about 130 nm. After deposition, the multilayer thin films were heated in the muffle at 500 °C for 70 h.

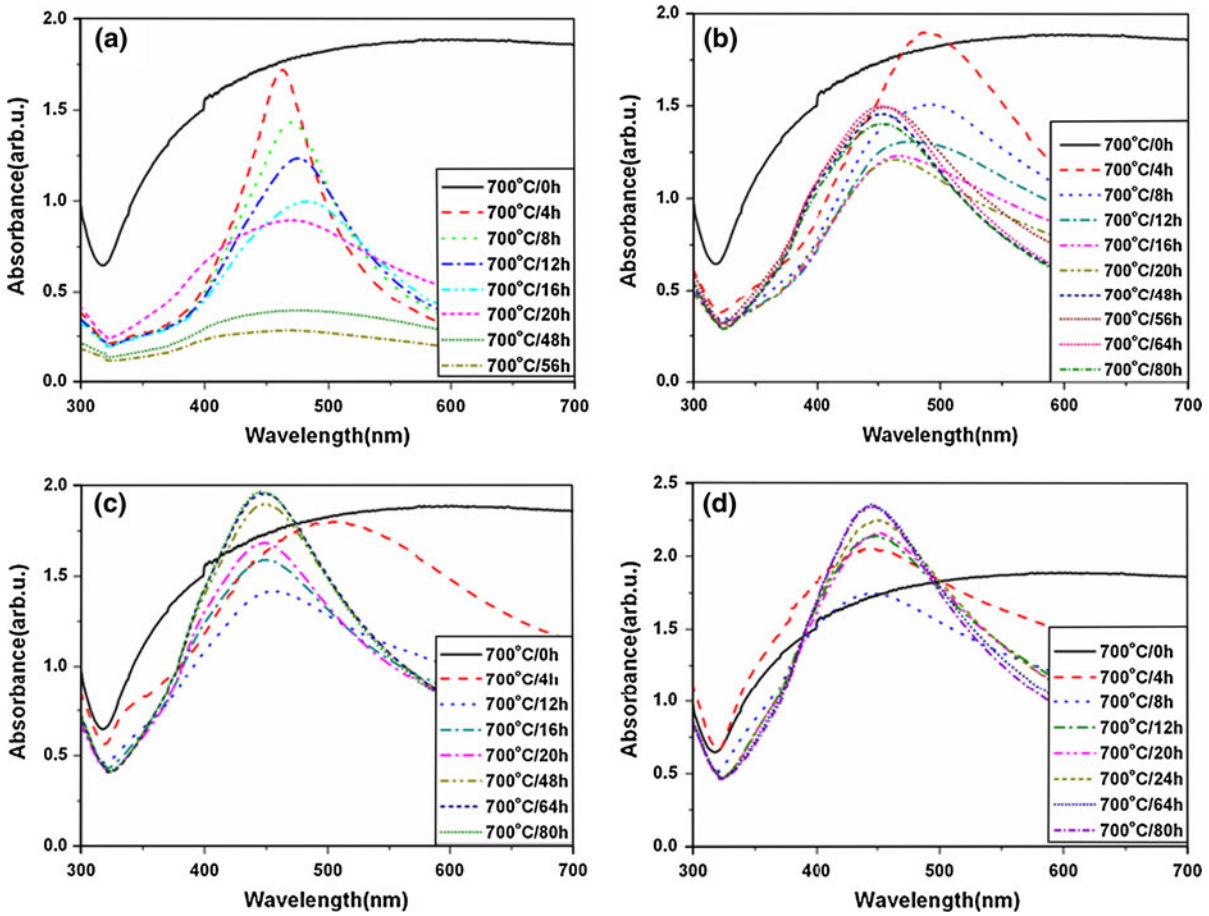

Fig. 1 The absorption spectra for samples annealed at 700 °C for different times. **a** Sample A, **b** sample B, **c** sample C, **d** sample D

Characterization

The absorption spectra of single layer Al_2O_3:Ag films were recorded on a dual-beam spectrophotometer (Jasco V-570) at normal incidence over the wavelength range of 300–700 nm. UV–Vis–NIR spectrum was obtained on the Perkin Elmer Lambda 750 spectrophotometer with an integrating sphere in spectral interval of 0.3–2.5 μm using $BaSO_4$ as a reference, while the infrared reflection spectra were obtained on the Bruker Tensor 27 spectrophotometer in the range of 2.5–25 μm without integrating sphere. High resolution transmission electron microscopy (HRTEM) equipped with an energy dispersive X-ray spectrometer (EDS) was used to study the composition, structure and morphology of thin films. The X-ray diffraction (XRD) patterns were obtained by the X'Pert Pro MPD with Cu Kα ($\lambda = 1.5408$ Å) at room temperature. The composition of thin film was also characterized by the X-ray photoelectron spectroscopy (XPS) (Kratos AXis Ultra (DLD)).

Results and discussion

The absorption spectra

The absorption spectra of samples annealed at 700 °C for different times are shown in Fig. 1. It can be found that there is a broad absorption peak at 597 nm of as-deposited thin films in the visible region, which origins from SPR of Ag nanoparticles. Further, the absorption spectra exhibited an absorption edge at 326 nm, which is due to the interband transition (Kreibig and Vollmer 1995). The absorption peak is broad, which is expected due to the inhomogeneous distribution of

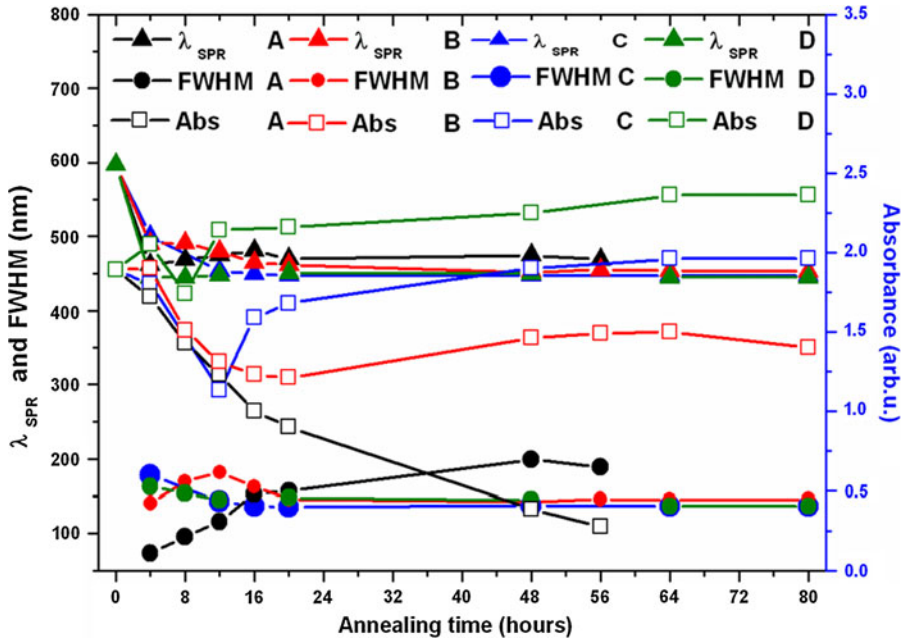

Fig. 2 The properties of absorption peak of samples annealing for different times

Ag nanoparticles including shape and size (Mandal et al. 2002). After annealing at 700 °C, the SPR absorption peak is fully changed. The absorption peak of Ag nanoparticles around 445–490 nm appears and the peak position (λ_{SPR}) is blue-shift compared with that of as-deposited samples (597 nm). The λ_{SPR} and full width of half maximum (FWHM) of absorption peak are compiled in Fig. 2. For sample A (60 nm), it is clearly shown that λ_{SPR} is around 470 ± 10 nm after annealing at different times. The FWHM of absorption peak broadens with the increase of annealing time. After annealing for 48 h, the FWHM of absorption peak is about three times as wide as that of samples annealing for 4 h, while the intensity of absorption peak (α) is sharply decreasing with the elongation of annealing time. For sample B (90 nm), the λ_{SPR} is apparently blue-shift from 491 to 452 nm with the increasing annealing time. When annealing time is longer than 48 h, the λ_{SPR} is almost constant around 453 ± 1 nm. The FWHM of absorption peak firstly broadens and then narrows with the increase of annealing time. The intensity of absorption peak is firstly decreasing with the increasing annealing time, while the intensity of absorption peak begins to increase when the annealing time is longer than 48 h. After annealing for 80 h, the intensity of absorption peak is slightly decreasing. For sample C (120 nm), the λ_{SPR} is blue-shift from 500 to 447 nm with the increasing annealing time. It becomes constant when annealing time is longer than 20 h. The FWHM of absorption peak firstly narrows with the increasing annealing time and then becomes constant after annealing for 16 h. The intensity of absorption peak is firstly decreasing and then increasing after annealing for 16 h. When the annealing time is longer than 64 h, the intensity of absorption peak is constant. For sample D (150 nm), the λ_{SPR} is around 448 ± 3 nm with different annealing times. The FWHM of absorption peak is firstly decreasing with the elongation of annealing time and becomes constant after annealing for 64 h. The intensity of absorption peak is increasing with the increasing annealing time and then becomes constant after annealing for 64 h.

The absorption peak is related with the shape, size, and amount of Ag nanoparticles and dielectric constant of matrix (Mandal et al. 2002; Dalacu and Martinu 2000; Lee et al. 1999). Considering the same annealing temperature and time, it can be found that the evolution of absorption peak is also dependent on the film thickness. The film thickness dependent thermal stability of absorption peak can be compiled in Table 1. It is clearly shown that the thermal stability of absorption peak is improved with the increase of film thickness. When single layer film thickness is smaller than 90 nm, the absorption peak can not be stable after annealing and it even can be extinct. While

Table 1 The stability time of absorption peak properties of samples after annealing

Sample	λ_{SPR} (nm)	FWHM (nm)	α (a.u.)
A (60 nm)	–	–	–
B (90 nm)	48 h	–	–
C (120 nm)	20 h	64 h	64 h
D (150 nm)	4 h	64 h	64 h

the single layer film thickness is larger than 120 nm, the absorption peak can be constant after annealing for 64 h, which means that the thermal stability of absorption peak can be controlled by film thickness. It is well known that absorption peak is resulted from the Ag nanoparticles and the thickness dependent variance of absorption peak is also resulted from the evolution of Ag nanoparticles. Therefore, the XRD, TEM, EDS, and XPS results are shown in the next part to investigate the evolution of Ag nanoparticles in sample A and D.

The XRD patterns

The XRD patterns of sample D (150 nm) with different annealing times are shown in Fig. 3. It can be found that only one weak peak at 44.5° is observed in as-deposited thin film. It is ascribed to the (002) plane of cubic Ag (JCPDS 04-0783) and the crystalline size according to Scherrer formula (Cullity 1978) is about 6 nm. After annealing for 8 h, the peak ascribed to Ag (002) plane is sharply increased with apparently preferential orientation. The crystalline size is about 57 nm. Simultaneously, another peak at 52° ascribed to Ag_2O (JCPDS 42-0874) appears, which means that some Ag nanoparticles are oxidized during annealing. The crystalline size of Ag_2O is about 7 nm. After annealing for 24 h, the peaks at 44.5° and 52° are both increased and the crystalline size of Ag and Ag_2O is about 140 and 42 nm, respectively. Moreover, another peak at 34.5° ascribed to (113) plane of Ag_2O is observed, which means that more Ag particles are transformed into Ag_2O. However, there is no peak ascribed to Al_2O_3 observed, which means that Al_2O_3 is amorphous during annealing.

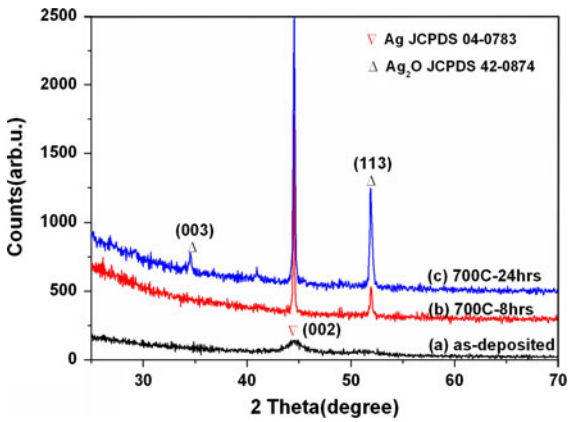

Fig. 3 The XRD patterns of sample D (150 nm)

The TEM images

To further investigate Ag nanoparticles, the TEM images of sample D are shown in Fig. 4. It can be found that the thickness is about 165 ± 10 nm which accords with the nominal thickness. According to the HRTEM image shown in Fig. 4b, the spacing of crystal lattice fringes on the black particles is about 2.05 Å, which is consistent with the interplanar crystal spacing of Ag (002) plane in XRD. The selective area electron diffraction (SAED) with diffuse rings in the inset of Fig. 4a means that the Ag nanoparticles are polycrystalline and the crystallinity is weak. Simultaneously, the distribution of Ag nanoparticles in Fig. 4a is extensive from 3–4 nm to 30–40 nm and the shape of Ag nanoparticles is not the regular sphere, which results in the SPR band broadening of as-deposited thin films (Lee et al. 1999). The crystalline size observed by TEM is different from that calculated by the XRD pattern. It may be the reason that the size calculated by XRD patterns is the crystalline size and the size observed by TEM is particle size. According to the EDS line scan of film thickness direction in Fig. 4c, it can be found that Al, O, and Ag elements are homogeneously distributed in the thin film.

After annealing for 8 h, the TEM images in Fig. 5 show that most of Ag nanoparticles are about 70 nm and the Ag particles about 3–4 nm are decreasing. It is related with the dissolution of smaller clusters and coarsening of larger ones by Ostwald ripening (Torrell et al. 2010). With the increasing annealing time, the upward diffusion of Ag nanoparticles results in the formation of bigger clusters. Thus, the average crystalline size calculated by XRD is close to the size observed by TEM images. Simultaneously, the shape of Ag nanoparticles approximates sphere, which

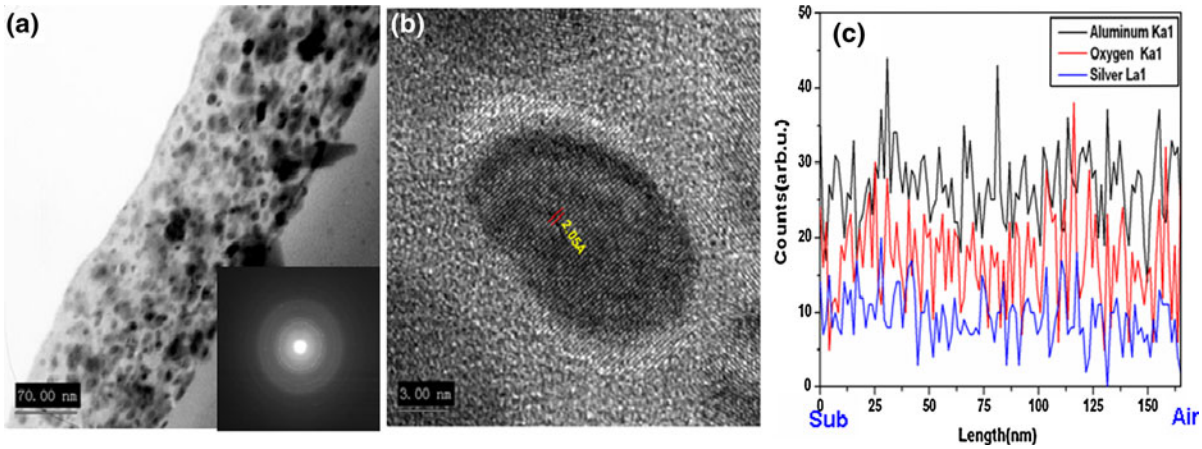

Fig. 4 TEM images of as-deposited thin film. **a** The cross-sectional TEM images and the SAED, **b** the HRTEM images of nanoparticles, **c** the EDS line scan of film thickness direction

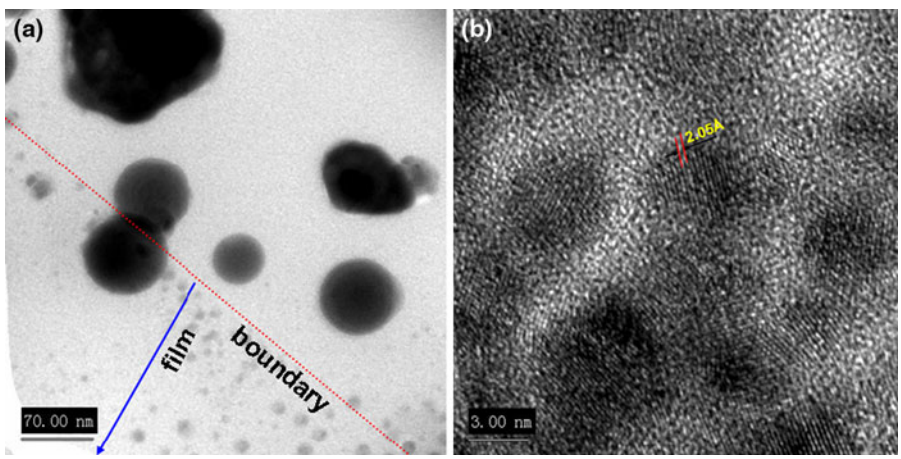

Fig. 5 TEM images of sample D annealing for 8 h. **a** TEM image, **b** HRTEM image

inevitably results in the FWHM of absorption peak narrowing in Fig. 1d (Mandal et al. 2002; Dong et al. 2009, 2010). The HRTEM images in Fig. 5b further prove the nanoparticles are cubic phase Ag particles.

In Fig. 6, the TEM images of sample D annealing for 24 h are shown. Through the cross-sectional image in Fig. 6a, it can be found that black particles adhere to the surface and cross-section of the thin film and the particle size is larger than 200 nm. The SAED in the inset of Fig. 6a illustrates that the particles are polycrystalline and the bright diffraction points prove that crystallinity is superior to sample annealing for 8 h. Through the HRTEM images in Fig. 6b, the crystal lattice fringe with a spacing of 2.05 Å corresponds to interplanar crystal spacing of Ag (002) plane, while the spacing of crystal lattice fringe about 2.5 Å corresponds to interplanar crystal spacing of Ag_2O (003) plane, which is consistent with the results in XRD patterns in Fig. 3. According to the EDS line scan of film thickness direction in Fig. 6c, it can be found that Al and O elements almost keep constant after annealing, while Ag is somewhat reduced comparing with that of as-deposited thin film. The distribution of Ag is somewhat increasing with film thickness, which further prove the upward diffusion of Ag during annealing. To further prove the existence of Ag_2O, the XPS results of thin film surface were shown in Fig. 6d. Through the high-resolution spectroscopy of Ag3d, it can be found that the binding energy of $Ag3d_{3/2}$ and $Ag3d_{5/2}$ are 371.8

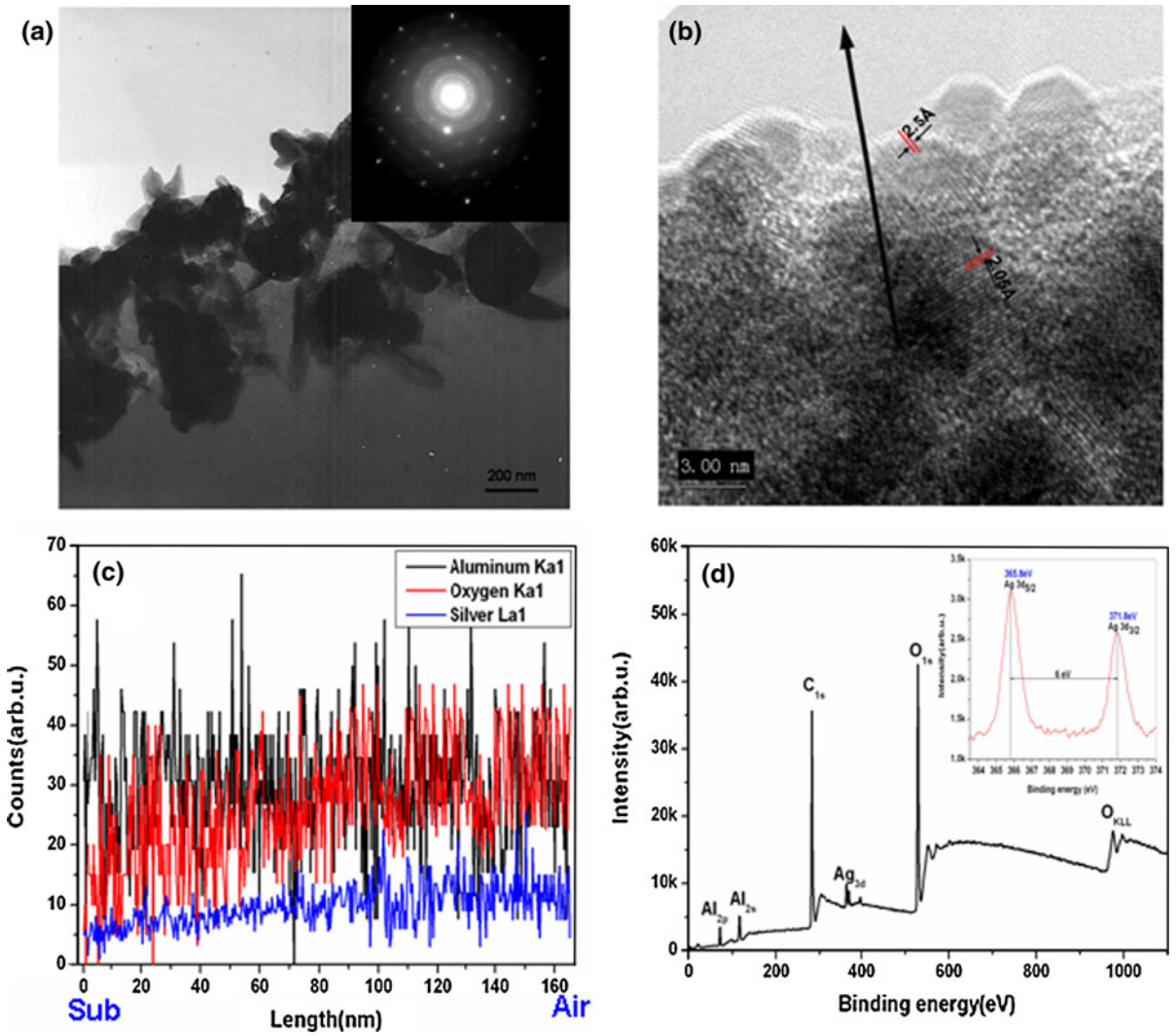

Fig. 6 TEM images of sample D annealing for 24 h. **a** The cross-sectional TEM image and the insert is SAED, **b** the cross-sectional HRTEM image, **c** the EDS line scan of film thickness direction, **d** the XPS survey of film surface and the insert is high-resolution spectroscopy of Ag3d

and 365.8 eV, respectively. It can be deduced that the Ag is existent as Ag oxide (Ag_2O) on the film surface (Wagner et al. 1979).Through the distribution of Ag_2O in HRTEM image, it can be found that the Ag_2O is out of the thin film surface, which means that Ag reacts with the oxygen in atmosphere.

In Fig. 7, the TEM images of sample A (60 nm) annealing for 8 h are shown. In Fig. 7a, it can be found that the nanoparticles are relatively small and most of the particles are smaller than 10 nm except for several particles larger than 10 nm. Moreover, the amount of Ag nanoparticles is increasing from surface to substrate. It is supposed that the melting point of Ag is decreasing with the decrease of particles size (Castro et al. 1990). The amount decrease of Ag near the surface may be due to the evaporation of Ag nanoparticles during annealing. According to the HRTEM images in Fig. 7b, the particles ascribed to Ag are also proved.

The TEM images of sample A annealing for 24 h are shown in Fig. 8. It can be found that there are only several big particles in the cross-section near the surface. The amount of Ag is apparently decreased considering the distribution of Ag nanoparticles. The

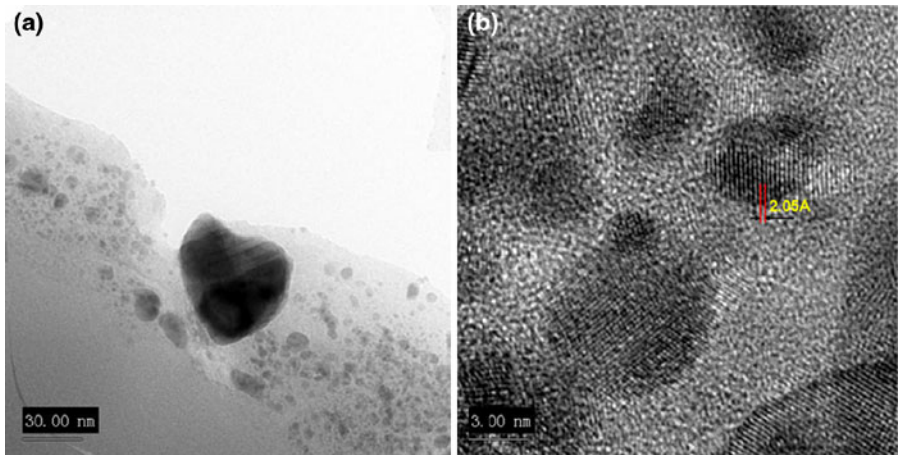

Fig. 7 TEM images of sample A annealing for 8 h. **a** The cross-sectional TEM image, **b** the HRTEM image

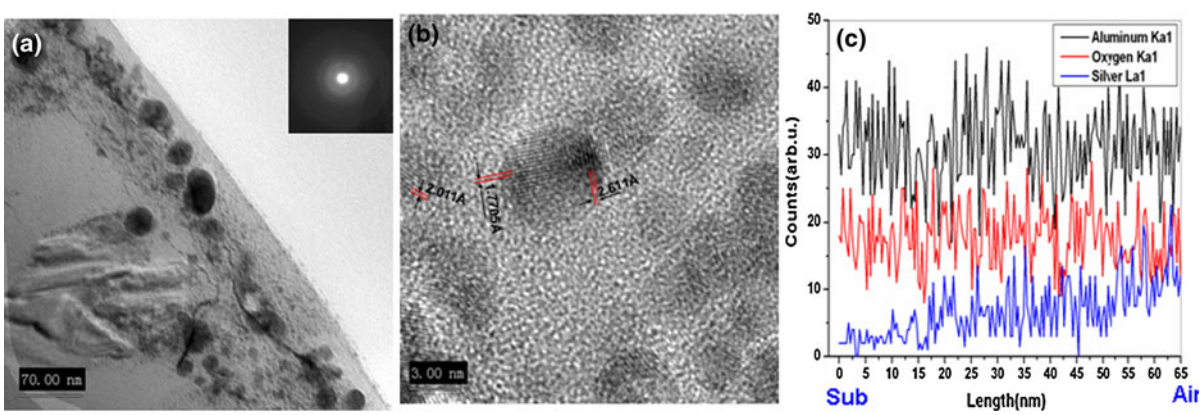

Fig. 8 TEM images of sample A annealing for 24 h. **a** The cross-sectional TEM image and the insert is SAED, **b** the HRTEM image, **c** the EDS line scan of film thickness direction

diffuse rings in the SAED of the inset in Fig. 8a illustrate that black particles are polycrystalline. According to the HRTEM images in Fig. 8b, it can be found that there are three kinds of crystal lattice fringe spacing observed. The fringe spacing about 2.011 Å is corresponding to the interplanar distance of Ag (002) plane, while the fringe spacing about 1.7705 and 2.611 Å correspond to the interplanar distance of Ag_2O (113) plane and (003) plane, respectively. According to the EDS line scan of film thickness direction in Fig. 8c, it can be found that the distribution of Al and O elements are almost the same as that of as-deposited thin film, while the distribution of Ag is greatly changed. After annealing for 24 h, the Ag amount is sharply reduced near the substrate and slowly augmented along film thickness direction. However, the intensity of Ag is apparently lower than that of as-deposited thin film, which means that the upward diffusion during annealing finally results in Ag evaporation into air.

The possible mechanism of absorption spectra evolution

Combined with the results of TEM and XRD, the evolution of absorption peak can be explained as following. Firstly, the shift of SPR band can be interpreted based on the Maxwell–Garnett effective medium theory (Castro et al. 1990; Xu et al. 2003, 2006, 2005). For simplicity, we only consider spherical metal nanoparticles. The SPR wavelength λ_{SPR} is given as

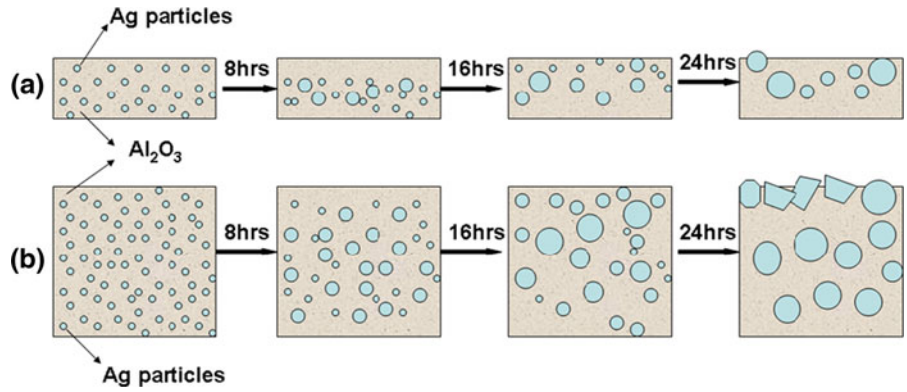

Fig. 9 The schematic illustration of the diffusion, agglomeration and evaporation of Ag particles in Al_2O_3:Ag thin films. **a** Sample A, **b** sample D

$$\lambda_{\mathrm{SPR}} = \lambda_p \left[\frac{2+q}{1-q}\varepsilon_{\mathrm{ext}} + 1\right]^{1/2} \quad (2)$$

where $\lambda_p = 2\pi c/\omega_p$ with $\omega_p = 9.2$ eV for Ag, q is the particle filling factor and $\varepsilon_{\mathrm{ext}}$ is the external dielectric constant surrounding the particles. From Eq. 2, one notes that λ_{SPR} is determined by two variables: $\varepsilon_{\mathrm{ext}}$ and q. An increase in $\varepsilon_{\mathrm{ext}}$ or q will make λ_{SPR} red-shift. During annealing at 700 °C, the diffusion in thin films is increased. The diffusion of Al_2O_3 can result in the densification of the matrix and result in the increase of dielectric constant. Considering the sputtering process, the void in the thin film is little and the densification is limited. Hence, the increase of dielectric constant resulted from densification can be neglected. The diffusion of Ag nanoparticles can result in the coarsening of particles, which is proved in the results of XRD and TEM. The melting point of metals is decreasing with the decreasing of particle size (Castro et al. 1990). De et al. (1996) and Arnold (1975) have ever reported that Ag nanoclusters begin to evaporate when annealing at 650 °C. During annealing, Ag nanoparticles on the surface can evaporate into the atmosphere and result in the amount of Ag is decreasing, which have ever been proved in cross-sectional TEM images and EDS line scan (Figs. 7, 8). Due to the decreasing amount of Ag particles, the λ_{SPR} can be blue-shift and the intensity of absorption peak can be reduced after annealing, which is consistent with the results shown in Fig. 1. However, the variance of Ag amount in thin films is dependent on the film thickness (Figs. 6, 8), which inversely influences the transformation of absorption peak. The evolution process of Ag particles during annealing can be given as the schematic illustration in Fig. 9.

During annealing at 700 °C, the Ag atoms can diffuse and the small particles can agglomerate and coarsen into big particles. The melting point of Ag nanoparticles is relatively lower than that of Ag bulk. Some nanoparticles near surface can diffuse and evaporate into atmosphere during annealing at 700 °C. When the film thickness is small (smaller than 60 nm), the diffusion path for Ag nanoparticles is finite and the upward evaporation is dominated, the agglomeration and coarsening is limited. With the increasing annealing time, the reduction of Ag amount is more and more apparent. Most of the small nanoparticles evaporate while only some big nanoparticles are retained. The decrease of Ag amount can greatly degrade the intensity of absorption peak (Fig. 1a). When the films thickness is large (larger than 150 nm), the diffusion path for Ag nanoparticles is long, coarsening and agglomeration is dominated, the size of Ag nanoparticles can be increased with the increase of annealing time. Except for evaporation of small particles, the big particles with high melting point can not be evaporated easily and the amount of Ag particles can not decrease on and on with increasing annealing time. Hence, the intensity of absorption peak can not be greatly changed and finally becomes constant (Fig. 1d). When the particles are small, surface energy is the main force to control the shape of particles and most of particles can be formed in sphere during annealing (Fig. 5a). When the particles are large enough, the shape is controlled by the crystal structure. Thus, the big particles with abnormal shapes adhere onto the film surface (Fig. 6a). Though the Ag_2O can be decomposed in high temperature (Barshilia et al. 2011; Bi et al. 2002), the cooling process can inevitably result in the oxidation of Ag particles on the surface and some

Ag_2O can be detected in thin film surface (Figs. 3, 6b, d). The size of Ag particles also has effect on the location, FWHM and the intensity of absorption peak. The size effect on absorption peak has two stages. At the first stage, the intensity of absorption peak increases while the absorption peak shifts to a shorter wavelength with the increasing size (Wilcoxon et al. 2001). At the second stage, the intensity of absorption peak continuously increases and there is no change in the location of absorption peak (Zhou et al. 2009). However, the particle size cannot be increased infinitely. When the Ag particles are large enough, not only the Ag particles can not be evaporated but the diffusion of the large particles is prevented. Hence, the intensity of absorption peak as well as the location of absorption peak is constant after annealing for enough long time (see Fig. 1d). Considering the variance of FWHM of absorption peak, the narrow distribution of particle size and regular sphere of Ag particles can result in the narrow bandwidth of absorption peak. The agglomeration and coarsening of Ag nanoparticles during annealing firstly result in the broad size distribution and then the big particles with similar size result in the constant bandwidth of absorption peak after long time annealing (see Fig. 1d).

The thermal stability analysis of multilayer thin films

The reflection spectra of multilayer thin films before and after annealing are shown in Fig. 10. It can be found that as-deposited Al_2O_3:Ag solar selective thin films have low reflectance around 0.3–2.5 μm and high reflectance around 2.5–25 μm. According to the reflection spectra, the absorptivity (α) and emissivity (ε) were calculated (Kennedy 2002; Uchino et al. 1979). The as-deposited thin films exhibited high absorptivity ($\alpha = 0.91$) in 0.3–2.5 μm region and low emissivity ($\varepsilon = 0.07$ at 25 °C) in 2.5–25 μm region, which illustrated that high solar selectivity is obtained in Al_2O_3:Ag thin films. After annealing, the reflection spectra are changed with two valleys appearance in 0.3–2.5 μm region and the point of minimal value shift near to 3 μm. The variation of reflection spectra is resulted from the evolution of Ag particles. After annealing, the diffusion and agglomeration of the Ag particles results in the decrease of absorption in absorbing layer and the interference in thin films becomes apparent, thus the two valleys appear, which can inversely result in high absorption. Simultaneously, the upward diffusion of Ag particles results the agglomeration of Ag particles on the surface, which could increase the reflectance in infrared region. The interference effects and increase of reflectance result in the shaper edge and blue-shift of reflection spectra in infrared region. The absorptivity and emissivity of thin films after annealing were 0.92 and 0.04, respectively, which means that the solar selectivity does not degrade and inversely is improved after annealing. The decrease of emissivity is resulted from the agglomeration of Ag particles on the surface as well as the increase of reflection in infrared region. Moreover, the appearance of thin films was not changed after annealing, which means that multilayer Al_2O_3:Ag thin film is appropriate as high-temperature solar absorbers.

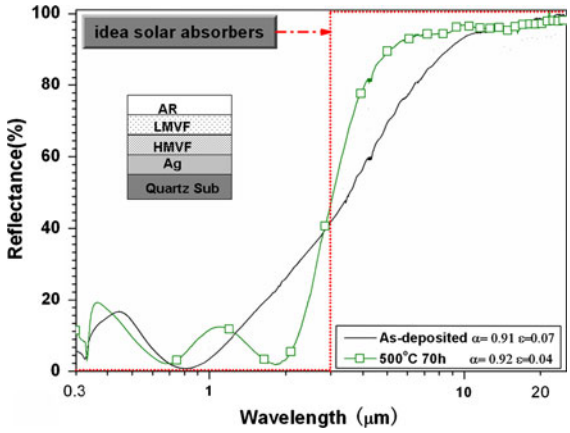

Fig. 10 The reflection spectra of multilayer Al_2O_3:Ag thin film before and after annealing at 500 °C for 70 h

Conclusion

Through the variance of SPR absorption, TEM images, XRD patterns, and composition analysis, the film thickness dependent thermal stability of the single layer Al_2O_3:Ag thin films after annealing at 700 °C are investigated. Due to the film thickness difference, the diffusion, agglomeration, and evaporation of Ag nanoparticles is different during annealing and the absorption peak is also greatly changed. When the thickness is smaller than 90 nm, the absorption peak can attenuate until extinct with the increasing annealing time due to the evaporation of Ag particles. While

the film thickness is larger than 120 nm, the absorption peak can be constant after annealing for 64 h. The solar selectivity of multilayer Al_2O_3:Ag solar selective thin films with absorbing layer thickness larger than 120 nm does not degrade after annealing at 500 °C for 70 h, which illustrates Al_2O_3:Ag thin film is a good candidate for high-temperature solar absorbers.

Acknowledgments This work was supported by the National Natural Science Foundation of China (Nos. 50876108 and 51102235) and Strategic New Industry Core Technology Research Project of Guangdong Province (2011A032304003) and CAS Key Laboratory of Renewable Energy and Gas Hydrate (No. KLREGHy007k6)

References

Arnold GW (1975) Near-surface nucleation and crystallization of an ion-implanted lithia–alumina–silica glass. J Appl Phys 46:4466–4470

Barshilia HC, Kumar P, Rajam KS, Biswas A (2011) Structure and optical properties of Ag-Al_2O_3 nano cermet solar selective coatings prepared using unbalanced magnetron sputtering. Sol Energ Mater Sol Cell 95:1707–1710

Bi HJ, Cai WP, Kan CX, Zhang LD (2002) Optical study of redox process of Ag nanoparticles at high temperature. J Appl Phys 92:7491–7495

Blain J, LeBel C, Saint-Jacques RG, Rheault F (1985) Spectrally selective surfaces of Co-pigmented anodic Al_2O_3. J Appl Phys 58:490–495

Cai WP, Zhong HC, Zhang LD (1998) Optical measurements of oxidation behavior of silver nanometer particle within pores of silica host. J Appl Phys 83:1705–1708

Castro T, Reifenberger R, Choi E, Andres RP (1990) Size-dependent melting temperature of individual nanometer-sized metallic clusters. Phys Rev Lett 42:8548–8553

Cullity BD (1978) Elements or X-ray diffraction. Addison-Wesley, Reading, MA

Dalacu D, Martinu L (2000) Temperature dependence of the surface plasmon resonance in Au/SiO_2 nanocomposites films. J Appl Phys 87:228–231

De G, Gusso M, Tapfer L, Catalano M, Gonella F, Mattei G, Mazzoldi P, Battaglin G (1996) Annealing behavior of silver, copper, and silver–copper nanoclusters in a silica matrix synthesized by the sol-gel technique. J Appl Phys 80:6734–6739

Dong G, Liu X, Xiao X, Qian B, Ruan J, Ye S, Yang H, Chen D, Qiu J (2009) Photoluminescence of Ag nanoparticle embedded Tb^{3+}/Ce^{3+} codoped $NaYF_4$/PVP nanofibers prepared by electrospinning. Nanotechnology 20:055707–055712

Dong G, Xiao X, Liu X, Qian B, Ma Z, Ye S, Chen D, Qiu J (2010) Preparation and characterization of Ag nanoparticle embedded polymer electrospun nanofibers. J Nanopart Res 12:1319–1329

Granqvist CG (1991) Materials science for solar energy conversion systems. Pergamon, Elmsford, NY

Kennedy CE (2002) Review of mid- to high- temperature solar selective absorber materials. NREL/TP-520-31267

Kelly KL, Coronado E, Zhao LL, Schatz GC (2003) The optical properties of metal nanoparticles: the influences of size, shape, and dielectric environment. J Phys Chem B 107:668–672

Kreibig U, Vollmer M (1995) Optical properties of metal clusters. Springer, Berlin

Lee M, Chae L, Lee KC (1999) Microstructure and surface plasmon absorption of sol–gel-prepared Au nanoclusters in TiO_2 thin films. Nanostruct Mater 11:195–199

Mandal SK, Roy RK, Pal AK (2002) Surface plasmon resonance in nanocrystalline silver particles embedded in SiO_2 matrix. J Phys D Appl Phys 35:2083–2198

Murray WA, Barnes WL (2007) Plasmonic materials. Adv Mater 19:3771–3778

Niklasson GA, Granqvist CG (1984) Optical properties and solar selectivity of co-evaporated Co-Al_2O_3 composites films. J Appl Phys 55:3382–3386

Peterson RE, Ramsey JW (1975) Thin film coating in solar thermal power system. J Vac Sci Technol A 12:174–179

Salmi J, Bonino JP, Bes RS (2000) Nickel pigmented anodized aluminium as solar absorbers. J Mater Sci 35:1347–1351

Sathiaraj TS, Thangarj R, Sharbaty AA, Bhatnagar M, Agnihotri OP (1990) Ni-Al_2O_3 selective cermet coatings for photo-thermal conversion up to 500°C. Thin Solid Films 190:241–244

Torrell M, Cunha L, Cavaleiro A, Alves E, Barradas NP, Vaz F (2010) Functional and optical properties of Au: TiO_2 nanocomposite films: the influence of thermal annealing. Appl Surf Sci 256:6536–6540

Uchino H, Aso S, Hozumi S, Tokumasu H, Yoshioka Y (1979) Selective surface of color-anodized aluminum for solar collectors. Natl Tech Rep 25:994–999

Wackelgard E, Chibuye T, Karlsson B (1990) North Sun '90, Solar Energy at High Latitudes (Reading, 1990). Oxford, Pergamon, p 177

Wagner C, Riggs W, Davis L, Moulder J, Muilenberg G (1979) Handbook of X-ray photoelectron spectroscopy. Perkin-Elmer Corporation, Eden Prairie, MN

Wang QH, Xu G, Xu XQ (2011) Study of Al_2O_3:Ag thin films as solar selective thin films. Acta Energ Solar Sinica (in chinese) 32:1748–1752

Wilcoxon JP, Martin JE, Provencio P (2001) Optical properties of gold and silver nanoclusters investigated by liquid chromatography. J Chem Phys 115:998–1001

Xu G, Tazawa M, Jin P, Nakao S, Yoshimura K (2003) Wavelength tuning of surface plasmon resonance using dielectric layers on silver island films. Appl Phys Lett 82:3811

Xu G, Tazawa M, Jin P, Nakao S (2005) Surface plasmon resonance of sputtered Ag films: substrate and mass thickness dependence. Appl Phys A: Mater Sci Process 80:1535–1538

Xu G, Chen Y, Tazawa M, Jin P (2006) Surface plasmon resonance of silver nanoparticles on vanadium dioxide. J Phys Chem B 110:2051–2055

Zhou LH, Zhang CH, Yang YY, Li BS, Zhang LQ (2009) Formation of Au nanoparticles in sapphire by using Ar ion implantation and thermal annealing. Nucl Instrum Methods B 267:58–62